Supporting Information for

Molecular dynamics simulation of local concentration and structure in multicomponent aerosol nanoparticles under atmospheric conditions

K.S. Karadima,[1,2] V.G. Mavrantzas,*[1,2,3] S.N. Pandis[1,2,4]

[1]Department of Chemical Engineering, University of Patras, Patras, GR 26504, Greece
[2]Institute of Chemical Engineering Sciences, FORTH-ICE/HT, Patras, GR 26504, Greece
[3]Department of Mechanical and Process Engineering, ETH-Z, Zürich, CH 8092, Switzerland
[4]Department of Chemical Engineering, Carnegie Mellon University, Pittsburgh, PA 15213, USA

All simulations have been carried out with the all-atom Optimized Potentials for Liquid Simulations (OPLS) force-field. [1] The total potential energy function is given as the sum of energies due to bond length stretching, bond angle bending, dihedral angles (torsional), and van der Walls (via Lenard-Jones potential function) and electrostatic (due to Coulombic forces) interactions:

$$U = U_{\text{stretching}} + U_{\text{bending}} + U_{\text{dihedral}} + U_{\text{VdW}} + U_{\text{electrostatic}} \quad \backslash\text{* MERGEFORMAT (S1)}$$

In OPLS no torsional interactions related with improper dihedrals are taken into account.[1] The functional form of the terms appearing in * MERGEFORMAT (S1) is as follows:

- $U_{\text{stretching}}$ is described by a harmonic potential function

$$U_{\text{stretching}} = k_{\text{stretching}} \left(l - l_0 \right)^2 \qquad \backslash\text{* MERGEFORMAT (S2)}$$

where $k_{\text{stretching}}$ describes the stiffness of the harmonic spring, l the bond length and l_0 the equilibrium bond length. Values of the parameters $k_{\text{stretching}}$ and l_0 for all types of bonds of the molecular species considered in our simulations are reported in Table S1.

- U_{bending} is also described by a harmonic potential function

$$U_{\text{bending}} = k_{\text{bending}} \left(\vartheta - \vartheta_0 \right)^2 \qquad \backslash\text{* MERGEFORMAT (S3)}$$

where k_{bending} denotes the stiffness of the harmonic spring used to model angle bending, ϑ the value of the bond angle and ϑ_0 the equilibrium value of the bond angle. Values of the parameters k_{bending} and ϑ_0 for all bond angles of the molecules considered in our simulations are reported in Table S2.

- U_{dihedral} is the potential function associated with contributions due to torsional angles for both skeletal and side atoms and is described by the following finite Fourier series

$$U_{\text{dihedral}} = \frac{V_1}{2}(1 + \cos\varphi) + \frac{V_2}{2}(1 - \cos 2\varphi) + \frac{V_3}{2}(1 + \cos 3\varphi) \quad \backslash\text{* MERGEFORMAT}$$

(S4)

where V_1, V_2 and V_3 are numerical parameters (their values are reported in Table S3) and φ denotes the dihedral angle.

- U_{VdW} denotes the potential energy due to intermolecular and intramolecular (non-bonded) interactions between all atom pairs separated by more than three bonds, with the exception of 1-4 interactions that are weighted with 0.5 (instead of 1.0 for all others). In the OPLS force field, a 12-6 Lennard Jones potential is employed

$$U_{\text{VdW}} = 4\varepsilon_{ij} \left[\left(\frac{\sigma_{ij}}{r_{ij}} \right)^{12} - \left(\frac{\sigma_{ij}}{r_{ij}} \right)^6 \right] \qquad \backslash\text{* MERGEFORMAT (S5)}$$

where ε is the depth of the potential well and σ the distance at which the intermolecular potential between the two particles/atoms i and j is zero. Their values for all types of atoms appearing in the systems addressed in our work are summarized in Table S4. For different atomic pairs ij, the corresponding σ and ε parameters were estimated by using the geometric mixing rule (see Equation * MERGEFORMAT (S8)).

- $U_{electrostatic}$ describes the potential energy due to electrostatic interactions between charged atoms. Like the Lennard-Jones interactions, only intermolecular and intramolecular (non-bonded) interactions between pairs of atoms separated by more than three bonds (with the exception of 1-4 interactions that are weighted by 0.5) are taken into account. It is given by the following form:

$$U_{electrostatic} = \frac{1}{4\pi\varepsilon_0}\frac{q_i q_j}{r_{ij}}$$

* MERGEFORMAT (S6)

where q is the atomic charge value, r the distance between the two charged atoms and ε_0 the permittivity of free space. All atomic charges needed to calculate $U_{electrostatic}$ are defined in Table S4.

We also used the following switching function, $S(r)$, for the Lennard-Jones potential: [2]

$$S(r) = \begin{cases} 1 & , r \leq r_{in} \\ \dfrac{\left(r_{out}^2 - r^2\right)^2 \left(r_{out}^2 + 2r^2 - 3r_{in}^2\right)}{\left(r_{out}^2 - r_{in}^2\right)^3} & , r_{in} < r < r_{out} \\ 0 & , r \geq r_{out} \end{cases}$$

* MERGEFORMAT (S7)

providing a smooth transition to the zero value between an inner, r_{in}, and an outer, r_{out}, cut-off (12 Å and 14 Å, respectively in this study) radius, where r is the distance between the two atoms. Regarding the geometric mixing rule for pair coefficients of the Lennard-Jones parameters between different types of atoms adopted, according to OPLS: [1]

$$\varepsilon_{ij} = \left(\varepsilon_i \varepsilon_j\right)^{1/2}$$
$$\sigma_{ij} = \left(\sigma_i \sigma_j\right)^{1/2}$$

* MERGEFORMAT (S8)

Table S1 Force field parameter values for the bond-stretching interactions. The notation is explained in Table S5

Bond type	$k_{stretching}$ (kcal mol^{-1} Å^2)	l_0 (Å)	Bond type	$k_{stretching}$ (kcal mol^{-1} Å^2)	l_0 (Å)
CY-CY	260	1.520	CY-CT	280	1.510
CY-HC	340	1.088	CT-CT	268	1.529
C-CY/CT, RCO	317	1.522	CT-HC	340	1.090
C-O, RCO	570	1.229	S-O, SO$_4^{2-}$	700	1.527[3]
C-OH, RCOOH	450	1.364	N-H, NH$_4^{1+}$	434	1.010
OH-HO, RCOOH	553	0.945	O-H, H$_2$O[4]	450	1.000
C-CT, RCOOH	317	1.522	N-N, N$_2$	450	1.100[5]
C-O, RCOOH	570	1.229	O-O, O$_2$	450	1.210[5]

Note: For the bond between a CY atom and a C atom of RCO, we used the same parameter values as for CT atoms.

Table S2 Force field parameter values for the bond angle bending interactions. The notation is explained in Table S5

Bond angle type	$k_{bending}$ (kcal mol^{-1} rad^2)	ϑ_0 (deg)	Bond angle type	$k_{bending}$ (kcal mol^{-1} rad^2)	ϑ_0 (deg)
CY-CY-CY	30.00	83.00	CT-CY-HC	35.00	114.30
CY-CY-HC	37.50	117.20	CY-CT-HC	37.50	110.70
HC-CY-HC	35.00	114.30	HC-CT-HC	33.00	107.80
CY-CY-CT	37.50	117.20	CT-CT-CT	58.35	112.70
CT-CY-CT	35.00	114.30	CT-CT-HC	37.50	110.70
CY-CY-C, RCO	63.00	111.10	CY-CT-C, RCOOH	63.00	111.10
HC-CY-C, RCO	35.00	109.50	CT-C-O, RCOOH	80.00	120.40
HC-CT-C, RCO	35.00	109.50	C-CT-HC, RCOOH	35.00	109.50
CY-C-CT, RCO	70.00	116.00	CT-C-OH, RCOOH	70.00	108.00
CY/CT-C-O, RCO	80.00	120.40	O-S-O, SO$_4^{2-}$	119.00	109.50[3]
O-C-OH, RCOOH	80.00	121.00	H-N-H, NH$_4^{1+}$	43.60	109.50
C-OH-HO, RCOOH	35.00	113.00	H-O-H, H$_2$O[4]	55.00	109.47

Note: For bond angles that involve a CY atom and a C atom of RCO or RCOOH, we used the same parameter values as for CT atoms.

Table S3 Force field parameter values for the torsional (dihedral angles) interactions. The notation is explained in Table S5

Dihedral angle type	V_1 (kcal mol^{-1})	V_2 (kcal mol^{-1})	V_3 (kcal mol^{-1})
CY-CY-CY-CY	0.000	0.000	0.000
CY-CY-CY-HC	0.000	0.000	0.000
HC-CY-CY-HC	0.000	0.000	0.000
CY-CY-CY-CT	0.000	0.000	0.000
CT-CY-CY-CT	0.000	0.000	0.000
CT-CY-CY-HC	0.000	0.000	0.000
CY-CY-CT-HC	0.000	0.000	0.300
CT-CY-CT-HC	0.000	0.000	0.300
HC-CT-CY/CT-HC	0.000	0.000	0.300
HC-CT-CT-CT	0.000	0.000	0.300
CT-CT-CT-CT	1.300	-0.200	0.200
CY/CT-CY-CY-C, RCO	-1.697	-0.456	0.585
CT-C-CY-CY, RCO	1.454	-0.144	-0.775
O-C-CY-CY, RCO	-0.277	1.228	-0.694
HC-CY-CY-C, RCO	0.000	0.000	-0.076
CT-C-CY-HC, RCO	0.000	0.000	0.275
CY-C-CT-HC, RCO	0.000	0.000	0.275
O-C-CY/CT-HC, RCO	0.000	0.000	0.000
HC-CY-CT-C, RCOOH	0.000	0.000	-0.100
OH-C-CT-CY, RCOOH	1.000	0.546	0.450
OH-C-CT-HC, RCOOH	0.000	0.000	0.000
CT-C-OH-HO, RCOOH	1.500	5.500	0.000
HO-OH-C-O, RCOOH	0.000	5.500	0.000
CY-CY-CT-C, RCOOH	-2.060	-0.313	0.315
O-C-CT-CY, RCOOH	0.000	0.546	0.000
O-C-CT-HC, RCOOH	0.000	0.000	0.000

Note: For dihedral angles that involve a CY atom and a C atom of RCO or RCOOH, we used the same parameter values as for CT atoms.

Table S4 Force field parameter values for the non-bonded (van der Walls and electrostatic) interactions. The notation is explained in Table S5

Atom type	q (e)	σ (Å)	ε (kcal mol^{-1})
CT,n-CH$_3$	-0.1800	3.5500	0.0660
CT/CY, RCH$_2$	-0.1200	3.5100	0.0660
CT, RCH	-0.0600	3.5000	0.0660
CT, RC	0.0000	3.5000	0.0660
HC, RH (n-alkane)	+0.0600	2.5000	0.0280
HC, RH	+0.0600	2.5000	0.0300
CY, RC	0.0000	3.4700	0.0770
CY, RCH	-0.0600	3.4700	0.0770
CY, RCH$_2$	-0.1200	3.4700	0.0770
CT, iso-CH$_3$	-0.1800	3.4100	0.0660
C, COR	+0.4700	3.7500	0.1050
O, COR	-0.4700	2.9600	0.2100
HC, CH$_n$COR	+0.0600	2.4200	0.0150
C, RCOOH	+0.5200	3.7500	0.1050
O=C, RCOOH	-0.4400	2.9600	0.2100
OH, RCOOH	-0.5300	3.0000	0.1700
HO, RCOOH	+0.4500	0.0000	0.0000
S, SO$_4^{2-}$	+2.0000[6]	3.5500[3]	0.2500[3]
O, SO$_4^{2-}$	-1.0000[6]	3.1500[3]	0.2000[3]
N, NH$_4^{+1}$	-0.4000	3.2500	0.1700
H, NH$_4^{+1}$	+0.3500	0.0000	0.0000
O, H$_2$O[4]	-0.8476	3.1656	0.1553
H, H$_2$O [4]	+0.4238	0.0000	0.0000
N, N$_2$[5]	0.0000	3.3100	0.0710
O, O$_2$[5]	0.0000	3.0900	0.0890

Table S5 Description of the notation used for the various types of atoms or groups

Atom type	Description
CT,n-CH$_3$	C atom in a straight chain alkane (terminals)
CT, iso-CH$_3$	C atom in an iso-branched alkyl group
CT, RCH$_2$/RCH/RC	C atom in an alkyl group with four substituents (either other alkyl group or hydrogen)
CY, RC/RCH/RCH$_2$	C atom in a cyclo-alkane with four substituents (either alkyl group or hydrogen)
HC, RH	H atom in an alkyl group
C, RCO	C atom in a ketone group
O, COR	O atom in a ketone group
HC, CH$_n$COR	H atom in alpha carbon of a ketone group
C, RCOOH	C atom in a carboxyl group
O=C, RCOOH	O atom (double bonded) in a carboxyl group
OH, RCOOH	O atom (single bonded, bonded with H) in a carboxyl group
HO, RCOOH	H atom in a carboxyl group
S, SO$_4^{2-}$	S atom in a sulfate anion
O, SO$_4^{2-}$	O atom in a sulfate anion
N, NH$_4^{+1}$	N atom in an ammonium kanion
H, NH$_4^{+1}$	H atom in an ammonium kanion
O, H$_2$O	O atom in a water molecule
H, H$_2$O	H atom in a water molecule
N, N$_2$	N atom in a nitrogen molecule
O, O$_2$	O atom in an oxygen molecule

A) The Cis-pinonic acid case
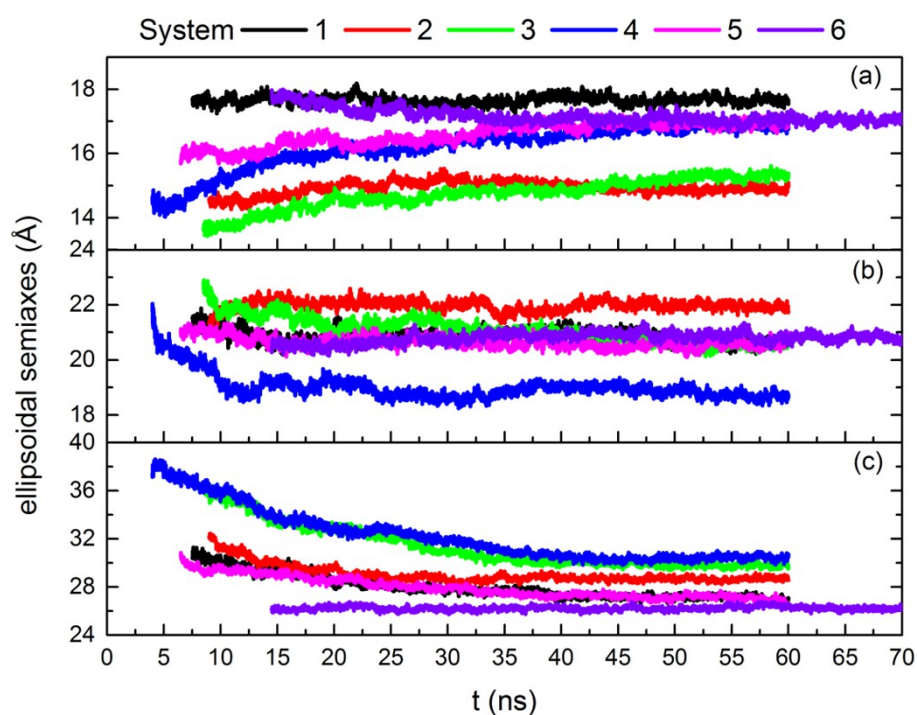
Fig. S1 Temporal evolution of the instantaneous values of the three ellipsoidal semiaxes: (a) 1st, (b) 2nd, and (c) 3rd of all simulated systems. The results are shown from the time the nanoparticle was formed.
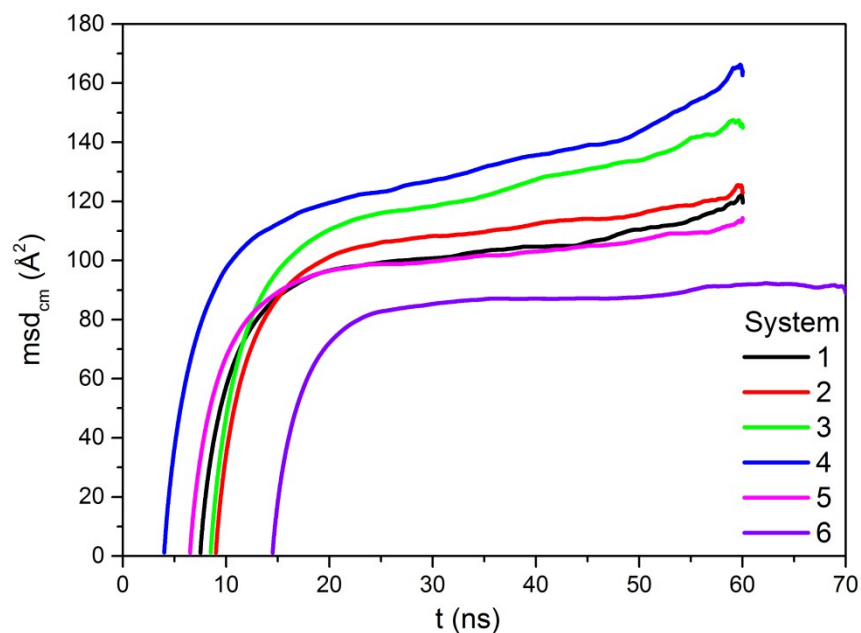
Fig. S2 Time evolution of the mean-square displacement between the centers-of-mass of all molecules or ions in the nanoparticle relative to their separation at the time the nanoparticle was formed, in the six different simulations.
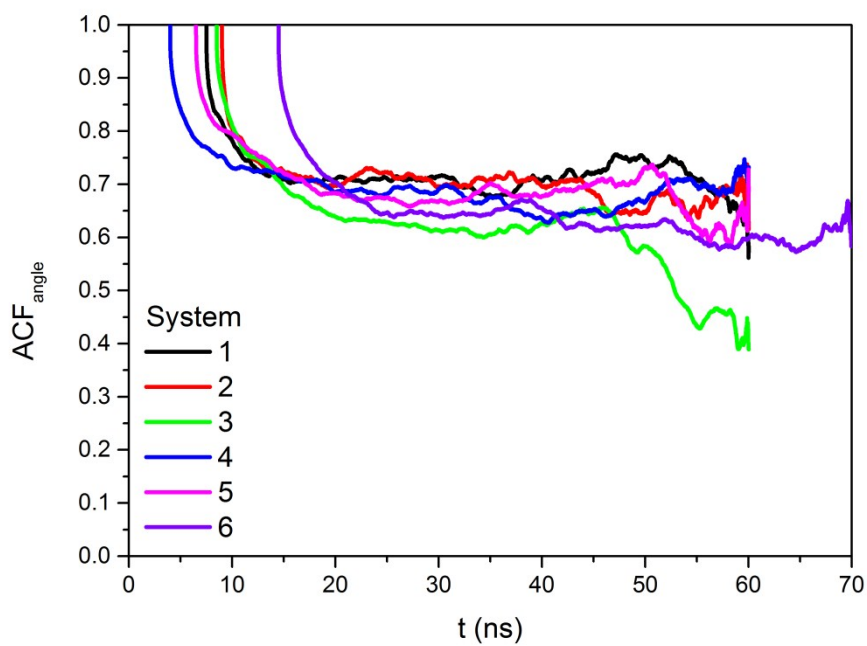
Fig. S3 Simulation results from the six different simulated systems for the time decay of the autocorrelation function ACF_{angle} corresponding to the angle formed by the position vectors of two different cpa molecules. System 3 (Table 1) displays a slightly different behavior at longer times due to a somewhat higher mobility of cpa molecules in comparison to the other systems.
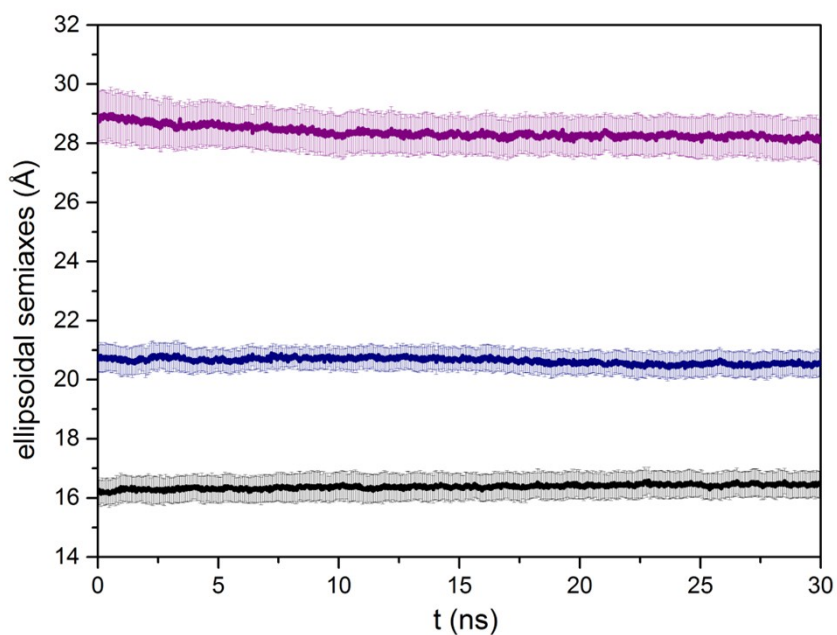
Fig. S4 Time evolution of the values of the three ellipsoidal semi-axes of the formed nanoparticle during the last 30 ns of the MD simulation, including standard errors of the mean.
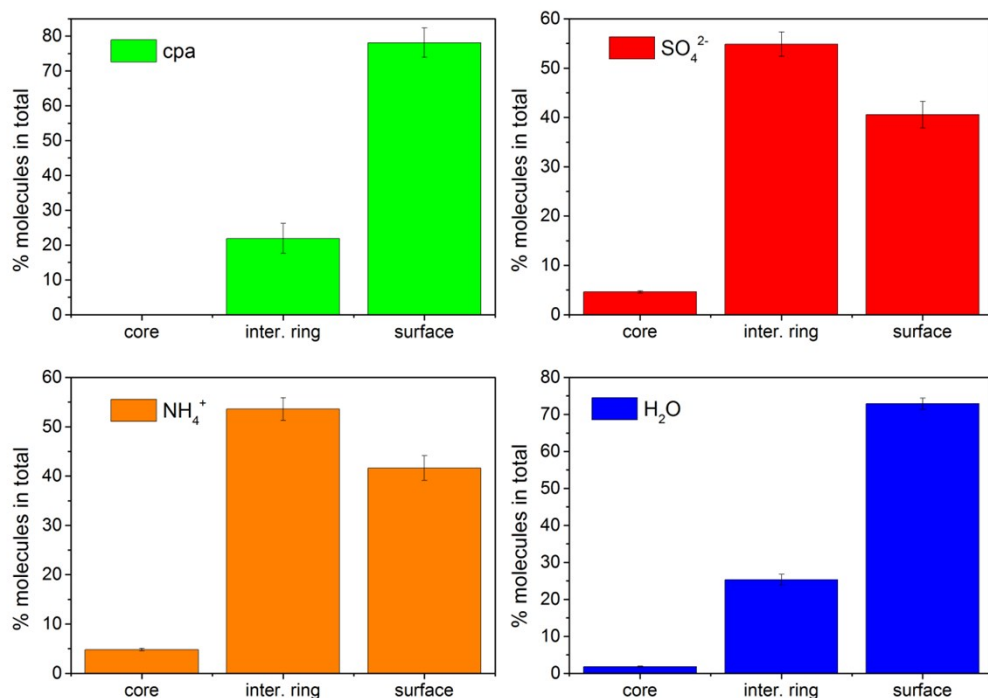
Fig. S5 Predicted percentages from the MD simulations of the number of the various chemical species in the three regions of the formed nanoparticle: the core, the intermediate ring, and the outer surface. Mean standard error bars are also included. All percentages have been calculated by averaging over time during the equilibrated part of the trajectory.
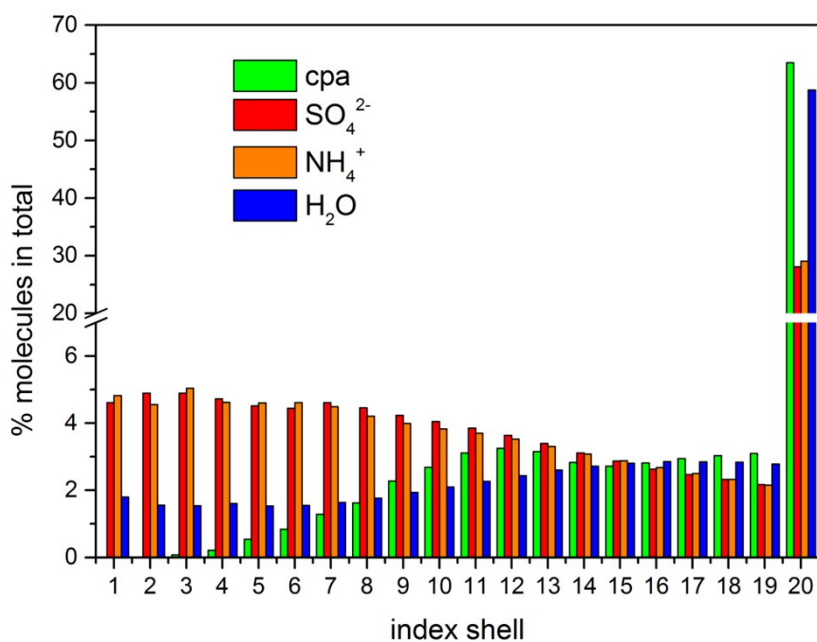
Fig. S6 Same as with Fig. S5 but with higher resolution inside the nanoparticle: the core (bin 1), the intermediate ring (bins 2-14), and the outer surface (bins 15-20).
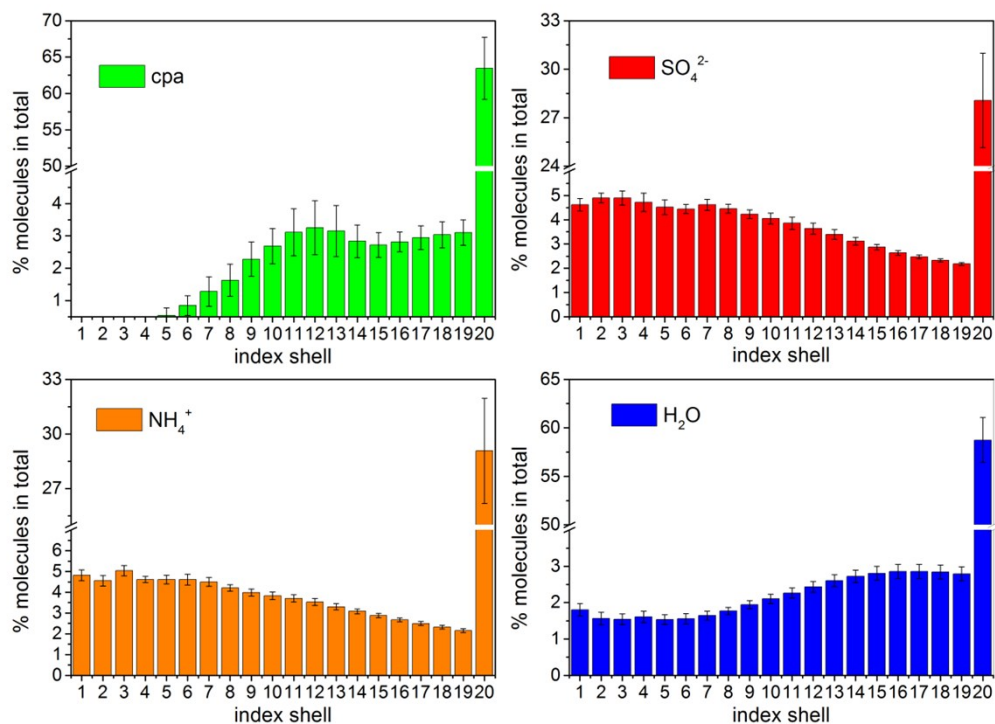
Fig. S7 Same as with Fig. S6 but with the results for the four different chemical species shown in separate graphs, including standard errors of the mean.
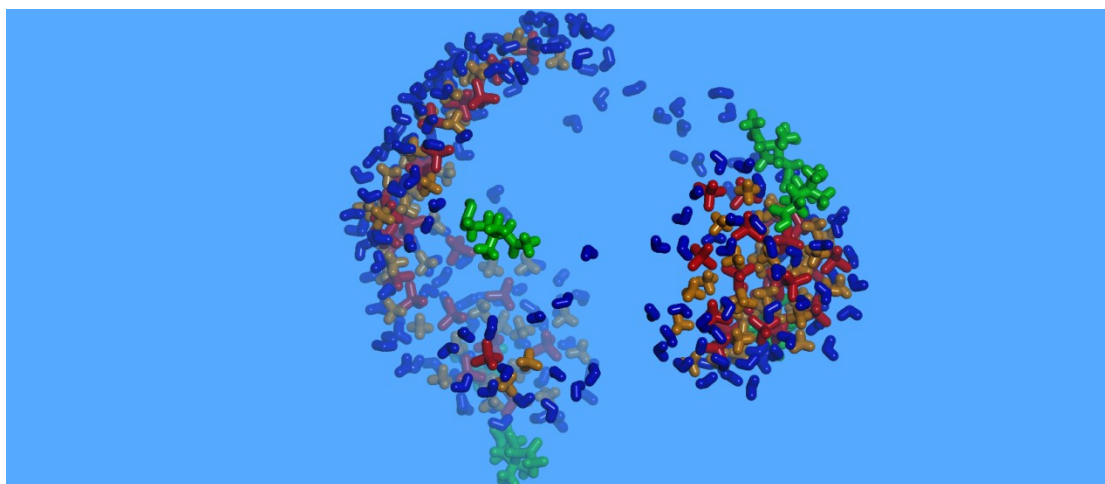
Fig. S8 Atomistic snapshot from the MD simulation with System 1 (Table 1) of the molecules/ions located in areas outside the perfect ellipsoid that approximates the formed particle at t = 60 ns. Depth perception is used for better visualization. Color notation: green for organic molecules, red for sulfate ions, orange for ammonium ions, blue for water molecules.
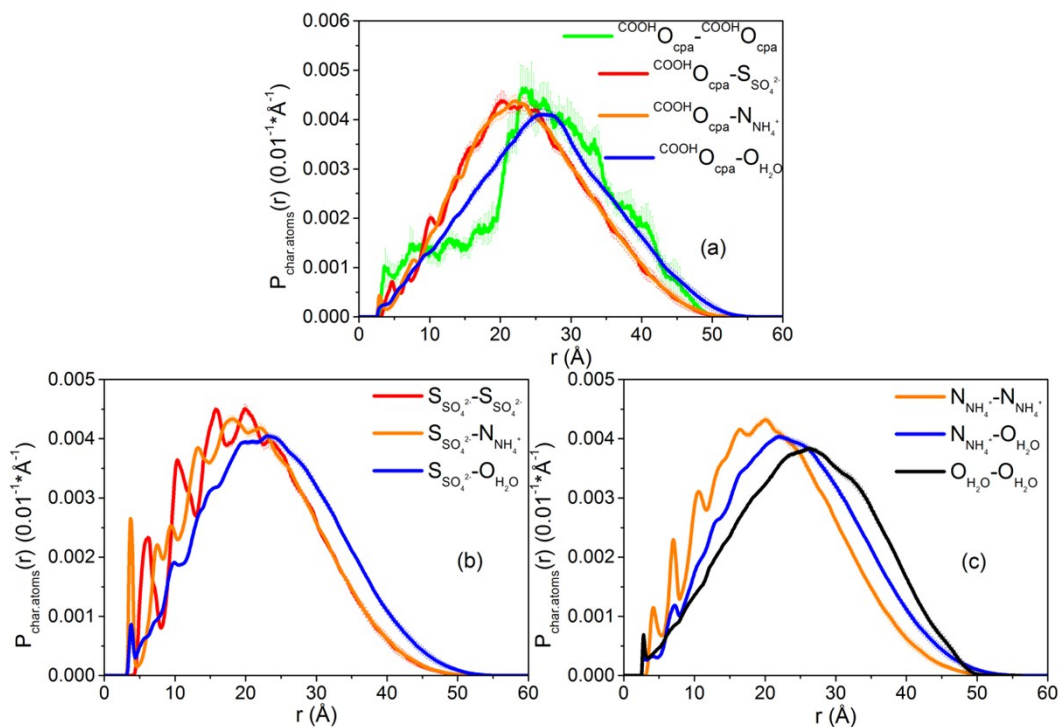
Fig. S9 Distribution of the distances between pairs of tagged atoms in the simulated nanoparticle, including standard errors of the mean. The strong peaks at the smallest distances in (b) confirm the solid-like state of the nanoparticle due to the strong binding of sulfate and ammonium ions. Standard errors of the mean are really small (almost indiscernible) for the distributions related with the inorganic species.
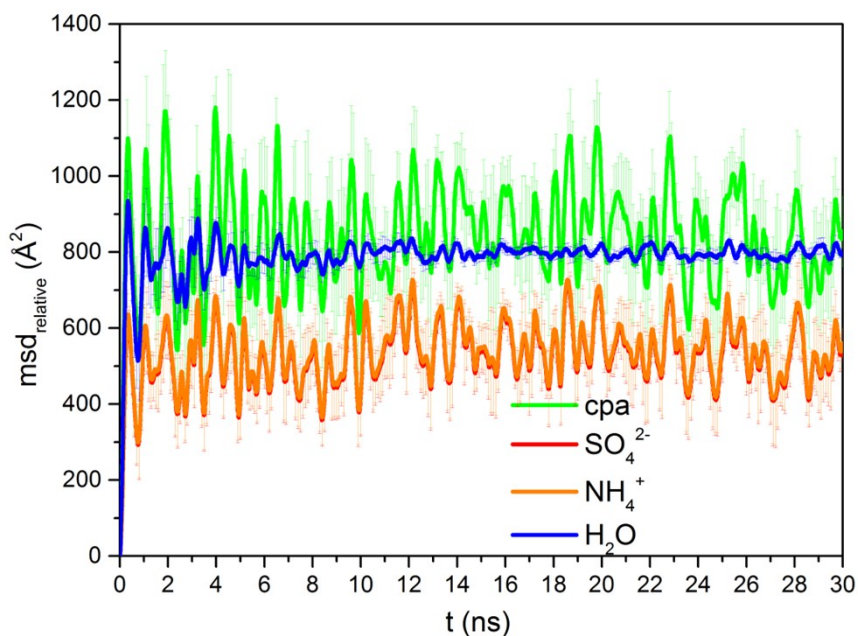
Fig. S10 Msd curves for the four different chemical species after having subtracted the motion of the center-of-mass of the nanoparticle. Error bars correspond to the standard error of the mean. Sulfate and ammonium ion displacements coincide, revealing their strong interaction.
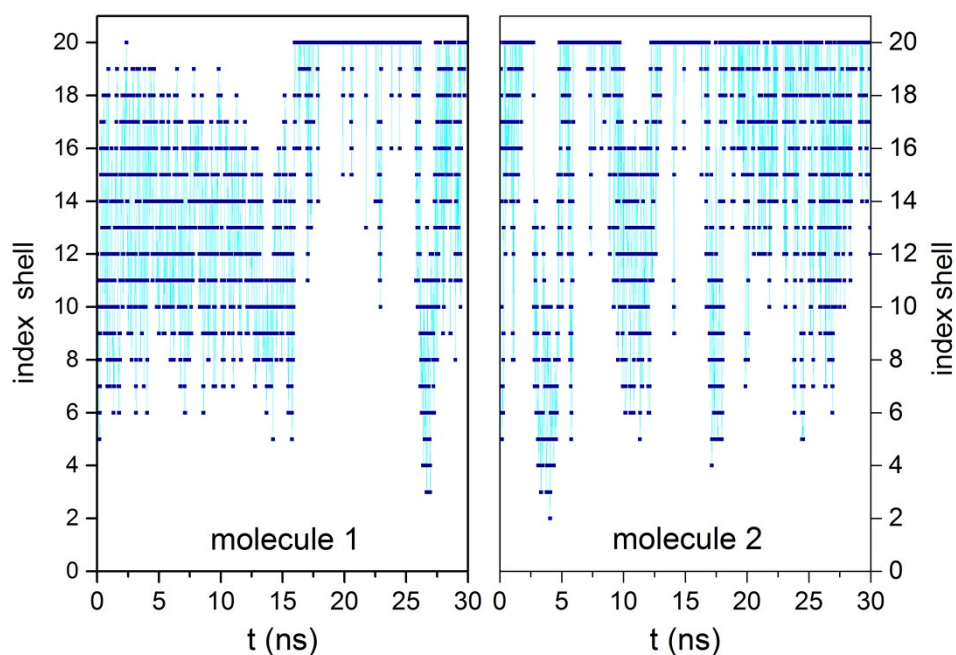
Fig. S11 Shells visited by two randomly selected water molecules in the course of the MD simulation with System 1 (Table 1). Similar (but not identical) graphs were obtained with all other water molecules and/or systems.
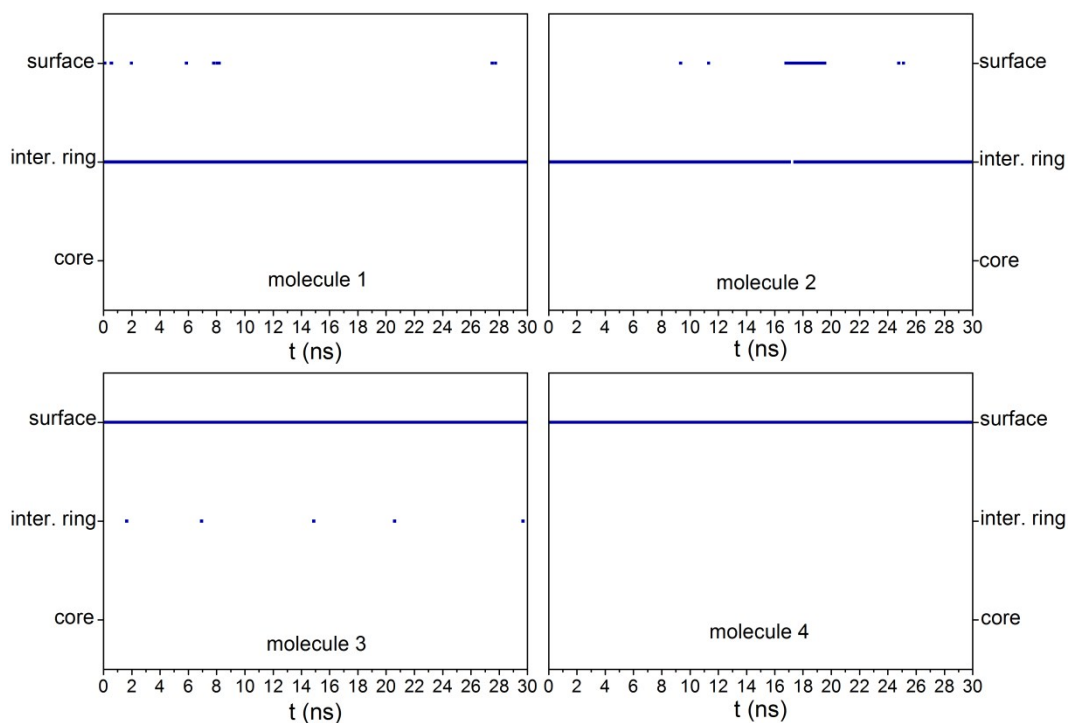
Fig. S12 Shells visited by four randomly selected cpa molecules in the course of the MD simulation with System 1 (Table 1). Similar (but not identical) graphs were obtained with all other cpa molecules and/or systems.

B) The n-triacontane case
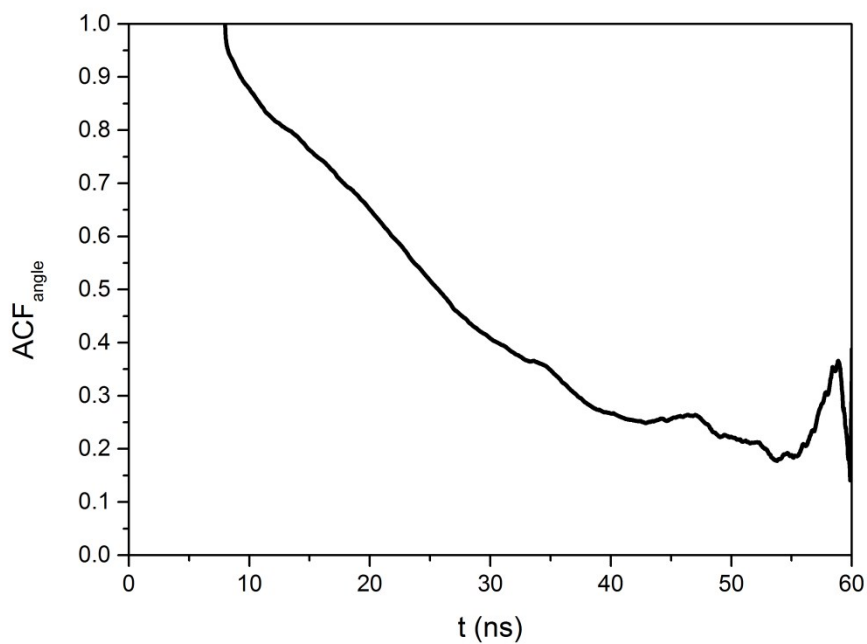
Fig. S13 Decay in time of the autocorrelation function ACF_{angle} corresponding to the angle formed by the position vectors of two different n-triacontane molecules.
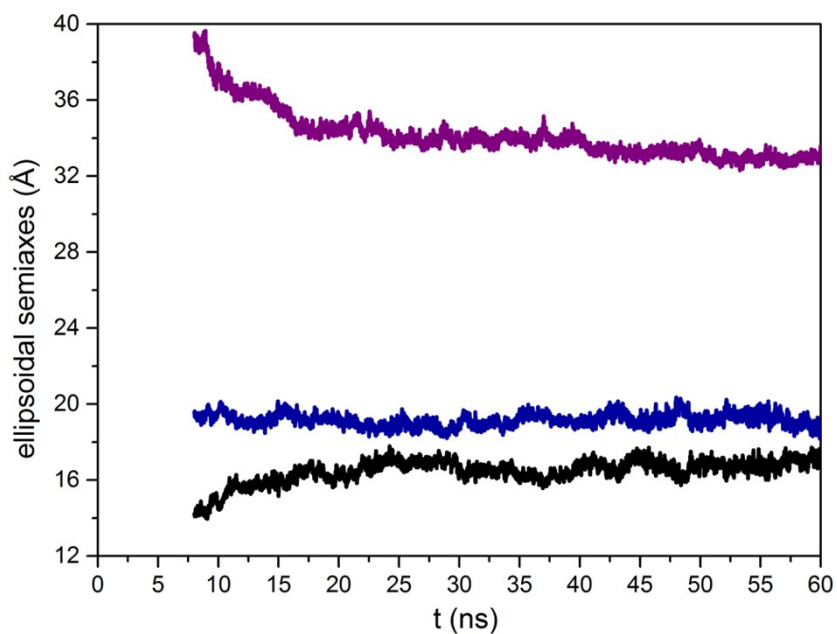
Fig. S14 Temporal evolution of the length of the three ellipsoidal semiaxes for the nanoparticle that contains n-triacontane molecules. The results are shown for times after the nanoparticle was formed.
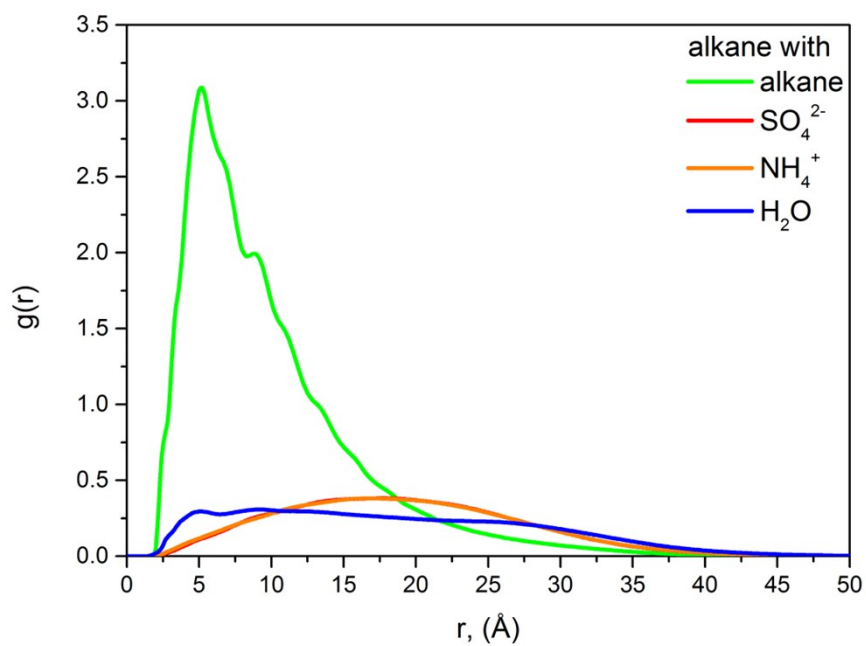
Fig. S15 Radial pair distribution functions between n-triacontane molecules and the rest of the chemical species in the nanoparticle.
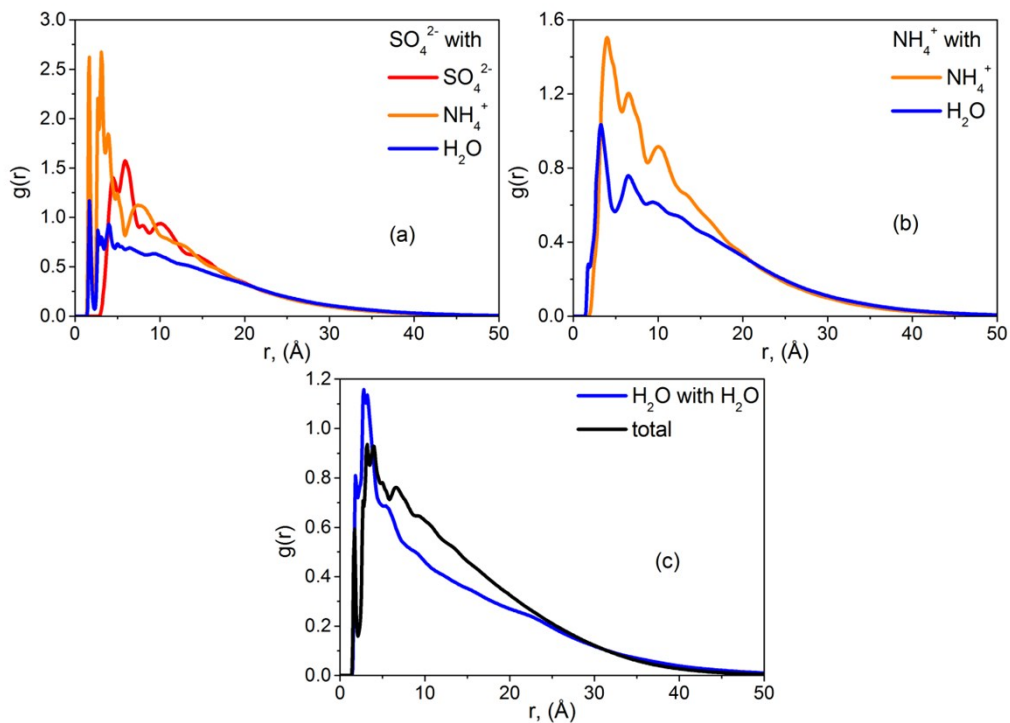
Fig. S16 Radial pair distribution functions of (a) sulfate ions, (b) ammonium anions, and (c) water molecules with other species except n-triacontane, as well as the total pair distribution function.
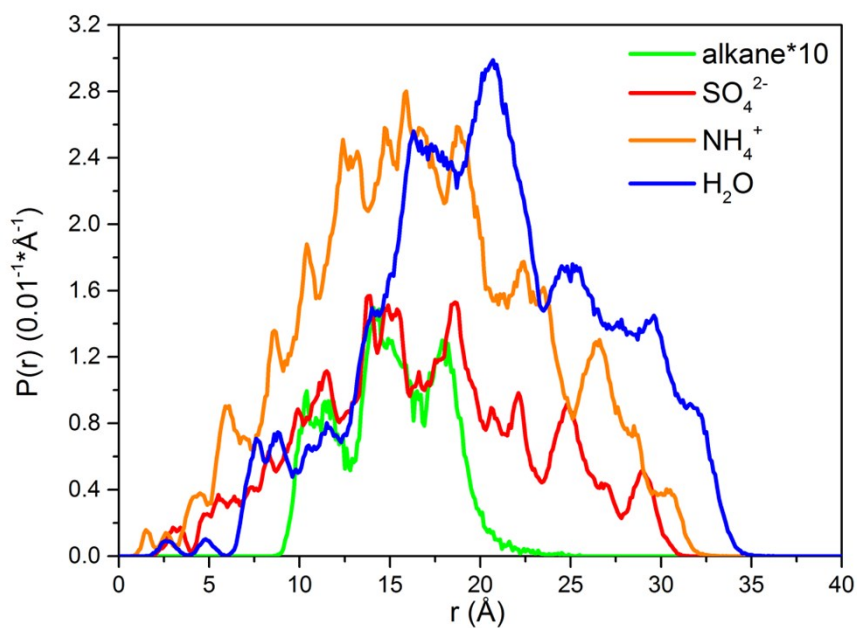
Fig. S17 Predicted distribution functions of the distances between the centers-of-mass of the four different chemical species from the center-of-mass of the nanoparticle. The result for n-triacontane has been magnified by a factor of ten (10).
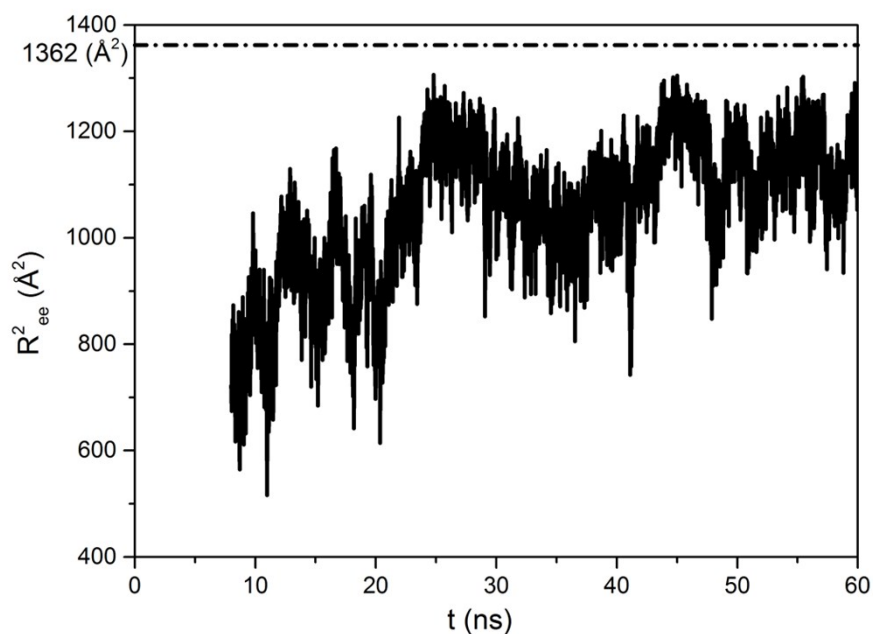
Fig. S18 Temporal evolution of the mean squared end-to-end distance vector of n-triacontane molecules. The dashed line marks the result for the all-trans configuration. The zero time coincides with the startup time of the MD simulation.
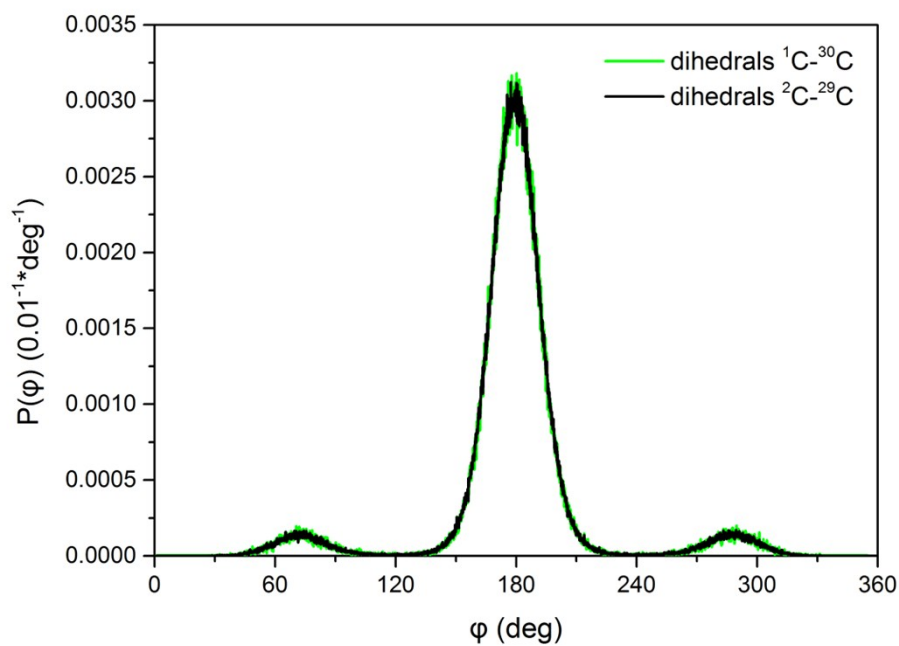
Fig. S19 MD predictions for the distribution of the dihedral angle C-C-C-C along the alkane backbone with (green line) without (black line) accounting for the two end carbon atoms that typically exhibit gauche defects.
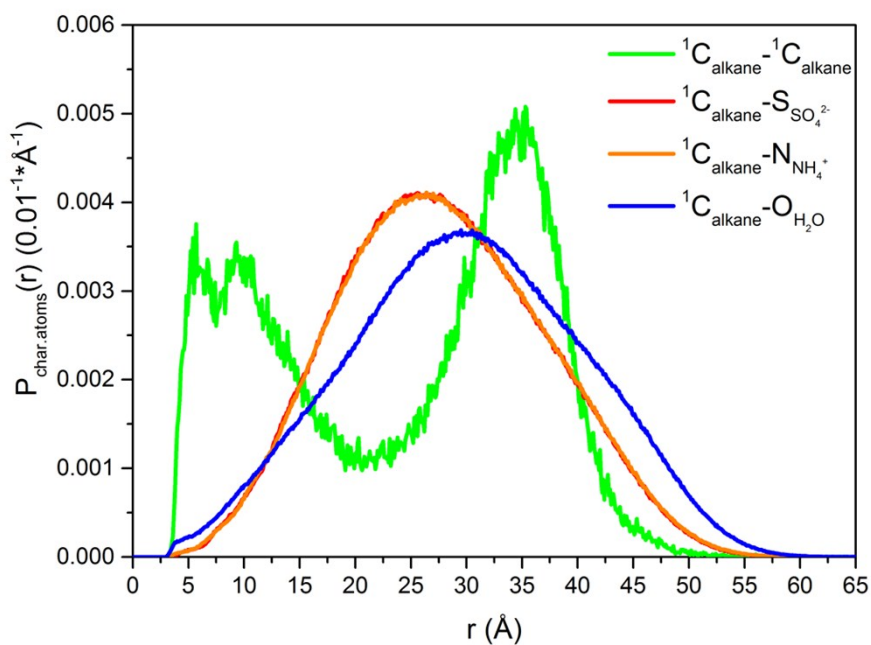
Fig. S20 Distribution function of the distances between pairs of different or similar species in the simulated nanoparticle. Tagged atoms: the first carbon atom (n-triacontane molecules), the sulfur atom (sulfates), the nitrogen atom (ammonium ion), and the oxygen atom (water molecules).
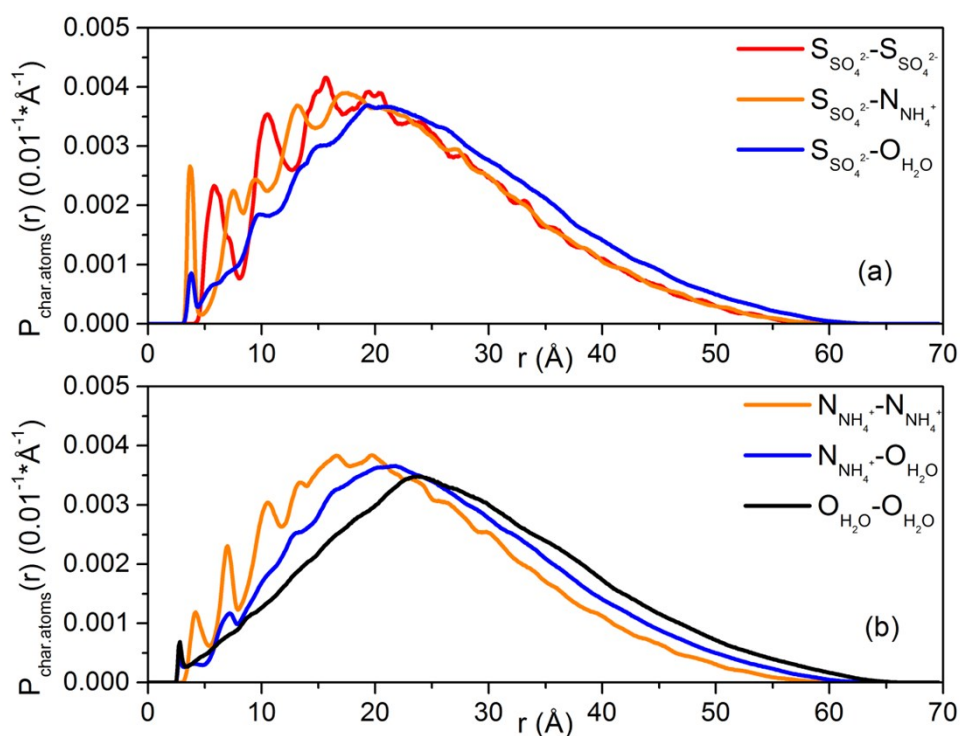
Fig. S21 Distribution functions of the distances between pairs of different or similar species (except n-triacontane molecules) in the simulated nanoparticle. Tagged atoms: the sulfur atom (sulfates), the nitrogen atom (ammonium ion), and the oxygen atom (water molecules). The results have been computed by averaging over time.
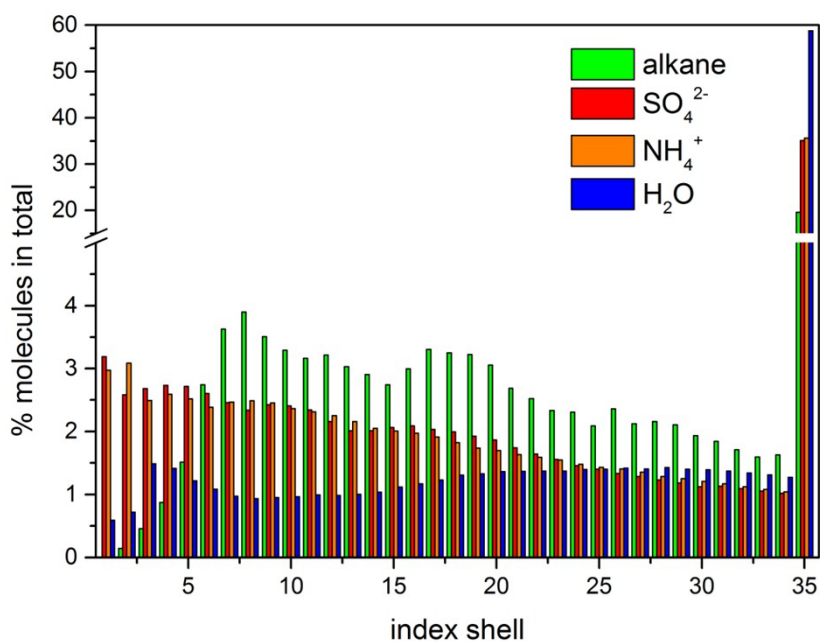
Fig. S22 Percentage of the number of the four different compounds in different regions inside the nanoparticle: the core (bin 1), the intermediate ring (bins 2-25), and the outer surface (bins 26-35). The results have been calculated by averaging over time.
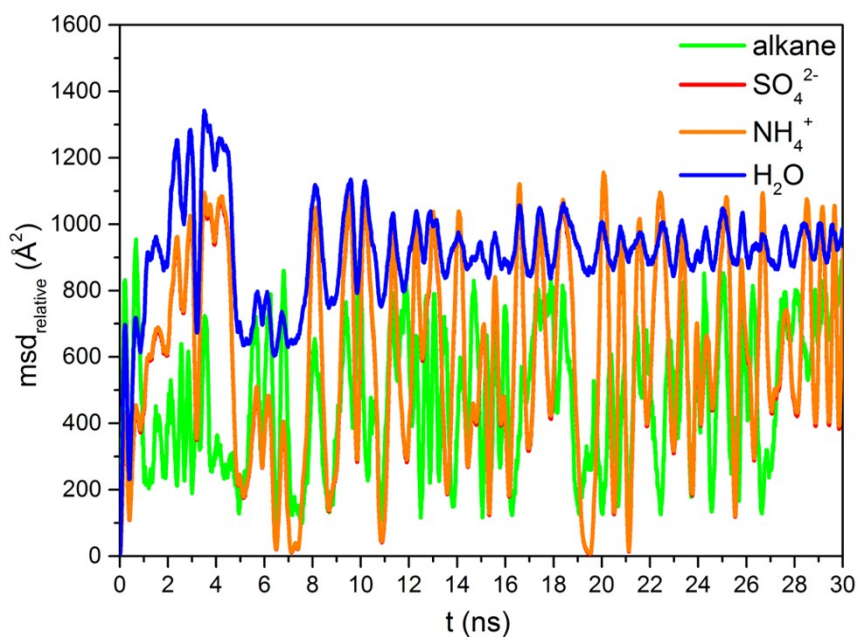
Fig. S23 Msd curves corresponding to the four different chemical species in the nanoparticle after having subtracted the motion of the nanoparticle itself, during the last 30 ns of the MD simulation. Sulfate and ammonium ion displacements coincide due to their strong binding.
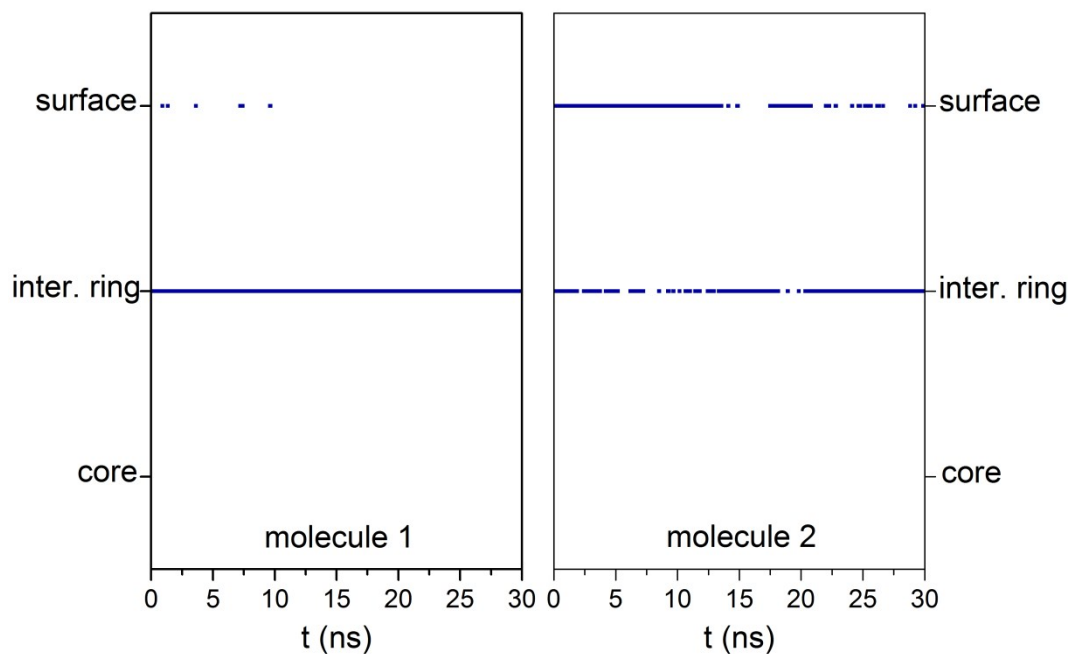
Fig. S24 Shells visited by two randomly selected n-triacontane molecules in the course of the MD simulation.

Supporting videos

Supporting video 1 (cpa particle formation) shows how newly formed nanoparticles move (translate and rotate) in the simulation cell subject to the imposed 3-d periodic boundary conditions (simulation System 1, see Table 1). The video corresponds to the first 12.50 ns of the simulation. Supporting video 2 (alkane particle structure) refers to the n-triacontane case and covers the first 20 ns after particle formation. To focus on the motion of organic molecules we have subtracted the displacement of the particle. The video zooms at the motion of the particle, and gas phase molecules have been removed for better visualization. In the course of the video, alkane molecules move from their initial positions and pack together, forming eventually a well-organized structure. In both videos, green refers to organic molecules (cpa or alkane), red and orange to sulfate and ammonium ions, respectively, and blue to water molecules. In video 1, light yellow is for nitrogen molecules and light grey for oxygen molecules.

BIBLIOGRAPHY

[1]   W. L. Jorgensen and J. Tirado-Rives, *J. Am. Chem. Soc.*, 1988, **110**, 1657–1666.
[2]   S. Plimpton, *J. Comput. Phys.*, 1995, **117**, 1-19, LAMMPS, http://lammps.sandia.gov/.
[3]   T. Ishiyama and A. Morita, *J. Phys. Chem. C*, 2011, **115**, 13704–13716.
[4]   H. J. C. Berendsen, J. R. Grigera and T. P. Straatsma, *J. Phys. Chem.*, 1987, **91**, 6269–6271.
[5]   G. Tsolou and V. G. Mavrantzas, Macromolecules, 2008, **41**, 6228–6238.
[6]   E. Wernersson and P. Jungwirth, *J. Chem. Theory Comput.*, 2010, **6**, 3233–3240.